Research Article | Vol. 28, No. 8 / 13 April 2020 / Optics Express 11482
Optics EXPRESS

Tunable multi-band terahertz absorber using a single-layer square graphene ring structure with T-shaped graphene strips

KAI-DA XU,[1,2,*] JIANXING LI,[1] ANXUE ZHANG,[1] AND QIANG CHEN[2]

[1]School of Information and Communications Engineering, Xi'an Jiaotong University, Xi'an 710049, China
[2]Department of Communications Engineering, School of Engineering, Tohoku University, Sendai 980-8579, Japan
[*]kaidaxu@ieee.org

Abstract: We numerically demonstrate a tunable dual-band terahertz metamaterial absorber (MA) with near-unity absorption using single-layer square graphene ring structure with T-shaped graphene strips. By periodically loading four T-shaped graphene strips to the square graphene ring periodic array without additionally increasing the size of MA device, the pre-existing resonant frequency will have a red shift and simultaneously a new resonance will be generated at higher frequency for achieving a dual-band MA. The two absorption peaks can be tuned to the resonant frequencies of interest by varying the parameters of the square graphene ring and T-shaped graphene strips. The operating frequency of the absorption spectrum can be also manipulated by adjusting the chemical potential of graphene, without changing their geometric parameters. Additionally, numerical results show that the proposed MA possesses polarization-independent and incident-angle-insensitive properties. To further extend the proposed structure's application with more absorption peaks, a tri-band MA is investigated through adding four more T-shaped graphene strips based on the dual-band absorber configuration. Therefore, our research work will be a good candidate for the design of various graphene-based tunable multi-band absorbers at different frequency regions with potential applications in optoelectronic devices and systems.

1. Introduction

Nowadays terahertz (THz) radiation ranging from 0.1 to 10 THz has been numerously applied in many engineering areas, such as imaging, sensing and communications [1–3]. As one of the most important devices in system applications, THz absorbers have been an attractive research topic recently, and metamaterial absorber (MA) has been intensively explored since the first theoretical and experimental demonstration of MA was presented by Landy et al. in 2008 [4,5]. In recent years, diverse MAs with different structures using periodic arrays have been deeply studied and developed [6–10], such as trapezoid arrays [6], square rings [7], cross resonators [8], split ring resonators [9] and all-dielectric metasurfaces [10], which aim to generate single-band, multi-band, or wideband perfect absorption.

Since the characteristics of the above metal-insulator-metal-based plasmonic MAs cannot be changed once fabricated, tunable MAs, based on two-dimensional materials including graphene [11,12], black phosphorus [13,14], and MoS_2 [15], have attracted increasing attentions accordingly. Among these materials, graphene has the highest carrier mobility and excellent mechanical properties. In addition, the complex conductivity of the graphene is tunable through changing the electrostatic doping or chemical doping [16]. A variety of graphene-based MAs with tunable absorption properties have been presented, primarily including broadband absorbers [17–21] and multi-band absorbers [22–28]. For the achievement of the multi-band absorption performance, three main design methods can be summarized. The first one is to utilize multilayer graphene

#390835 https://doi.org/10.1364/OE.390835
Journal © 2020 Received 20 Feb 2020; revised 26 Mar 2020; accepted 29 Mar 2020; published 2 Apr 2020

Optics EXPRESS

structures or graphene gratings such as the works in [22–25]. Methods in the second category rely on adding the metals or hBN above/beneath the graphene to construct a hybrid patterned structure [25–27]. These two above methods require multilayer configurations, which suffer from more complexity and difficulty of the MA's design and fabrication. The third approach is adding the number of the patterned graphene resonators in a periodic unit cell of the single-layer graphene in order to generate multiple resonances [28]. However, it will occupy relatively large size for the design of the periodic unit cell. From above, few works have paid attention to the investigation of new tunable multi-band THz MAs using single layer graphene and only one patterned resonator in a periodic unit cell [29,30], which can simplify the device fabrication technique and miniaturize the design simultaneously. In [29], a dual broadband THz absorber using electrical split ring resonator patterned graphene is proposed, but the polarization performance is sensitive under normal incident wave since the absorption curves of TM and TE polarizations have a frequency deviation of about 0.1 THz. In addition, a dual narrowband THz absorber is presented in [30], but the operating frequencies of the two absorption peaks cannot be flexibly tuned. Furthermore, all of these above-mentioned works are not easily extended to the absorber design with more absorption bands (e.g., tri-band absorber).

In this paper, we propose a terahertz MA to achieve tunable dual-band absorption characteristics, which consists of a single-layer periodically patterned graphene structure (square ring loaded with four T-shaped strips) and a metal ground plane spaced by polyethylene cyclic olefin copolymer (Topas) dielectric layer. The frequencies of two absorption peaks can be tuned by varying the parameters of the square graphene ring and T-shaped graphene strips as well as the chemical potential of graphene. Also, the dual-band MA can tolerate a wide range of incident angles with polarization-insensitive performance. To further extend the application of the proposed geometry with more absorption peaks, a tri-band MA is investigated through adding four more T-shaped graphene strips based on the above-mentioned dual-band absorber configuration.

2. Modeling and parameters

A schematic drawing of the proposed plasmonic dual-band metamaterial absorber is shown in Fig. 1. It is made up of a single-layer patterned graphene using a square ring structure loaded with four T-shaped strips, a dielectric layer using Topas with a relative permittivity of 2.35, and a ground plane using gold as a full reflective mirror. Topas is the trade name of a cyclic olefin copolymer (COC) manufactured by Topas Advanced Polymers GmbH in Germany, the U.S. and other countries [31]. As opposed to crystalline polyolefins as represented by conventional polyethylene (PE) and polypropylene (PP), it is an amorphous transparent copolymer possessing a cyclic olefin structure. It has some excellent properties, such as low loss for terahertz/optical signals, low birefringence, high Abbe's number, and high stiffness. A possible fabrication procedure for the proposed graphene-based dual-band THz absorber is described as follows. Firstly, the Topas layer on gold can be deposited by thermal evaporation. Then, a large scale graphene sheet grown on copper can be transferred on the Topas layer by the wet transfer technique [32,33]. By using oxygen plasma and electron-beam lithography (EBL), the patterned graphene is defined and the unwanted region is removed.

The absorption characteristics of the MA are investigated under periodic boundary conditions in the x-axis and y-axis directions using COMSOL Multiphysics, which is based on the finite element method (FEM) in the frequency domain. The FEM is a mathematical calculation method using numerical technique to obtain approximate solutions of problems in electromagnetics or physics. The incident terahertz plane wave is imposed downward from the top surface of MA. User-controlled tetrahedral meshes are applied in the whole computational domain. The frequency dependent absorption rate $A(\omega)$ can be expressed as $A(\omega) = 1 - R(\omega) - T(\omega)$, where the reflection $R(\omega)$ is equal to $|S_{11}(\omega)|^2$ and transmission $T(\omega)$ is expressed as $|S_{21}(\omega)|^2$. Since the gold mirror prevents the downward wave propagation, the transmission $T(\omega)$ can be seen

Optics EXPRESS

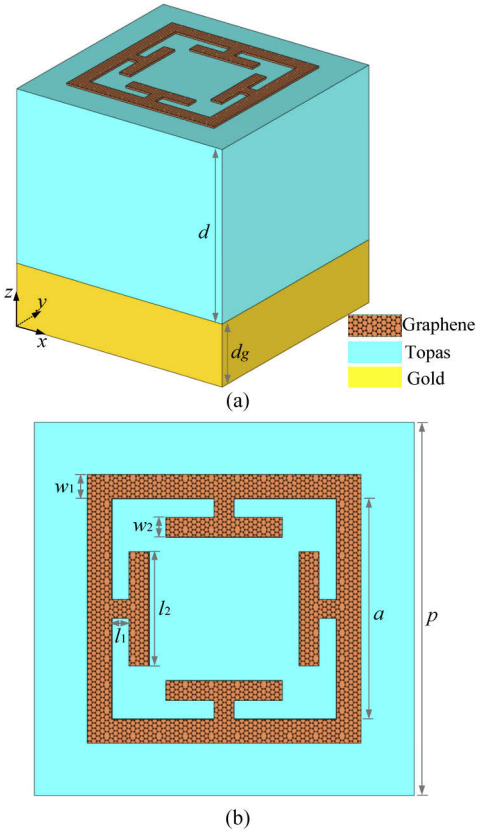

Fig. 1. (a) Perspective view and (b) top view of the proposed graphene-based dual-band terahertz absorber. The parameters w_1 and a are the widths and side lengths of the square graphene ring, respectively. The parameters w_2, l_1 and l_2 represent the width and two distinct lengths of the T-shaped graphene strips, respectively. d and d_g are the thicknesses of the spacer layers (Topas) and metal ground plane (gold), respectively. The symbol p is the periodicity of the periodic absorber structure. These parameters are set as: w_1=0.155 μm, w_2=0.12 μm, l_1 = 0.26 μm, l_2 = 1.1 μm, a=2.6 μm, p=4 μm, d=18 μm, and d_g=1 μm.

as zero over the entire frequency range of interest. Consequently, the absorption rate $A(\omega)$ will be $1 - R(\omega)$. Compared with the wavelength of incident wave, the thickness of graphene is neglectable, where the graphene can be treated as a 2D surface with zero thickness and isotropic surface conductivity.

The surface conductivity of graphene $\sigma(\omega)$ can be expressed by the following equations based on the Kubo formulas as below [34],

$$\sigma(\omega, \mu_c, \Gamma, \mathrm{T}) = \sigma_{\mathrm{intra}} + \sigma_{\mathrm{inter}} \tag{1}$$

$$\sigma_{\mathrm{intra}} = \frac{je^2}{\pi\hbar^2(\omega - j2\Gamma)} \int_0^\infty \xi \left(\frac{\partial f_d(\xi, \mu_c, T)}{\partial \xi} - \frac{\partial f_d(-\xi, \mu_c, T)}{\partial \xi} \right) d\xi \tag{2}$$

$$\sigma_{\mathrm{inter}} = -\frac{je^2(\omega - j2\Gamma)}{\pi\hbar^2} \int_0^\infty \frac{f_d(-\xi, \mu_c, T) - f_d(\xi, \mu_c, T)}{(\omega - j2\Gamma)^2 - 4(\xi/\hbar)^2} d\xi \tag{3}$$

$$f_d(\xi, \mu_c, T) = (e^{(\xi - \mu_c)/k_B T} + 1)^{-1} \tag{4}$$

Optics EXPRESS

where σ_{intra} and σ_{inter} are originated from the intraband and interband transition, respectively, f_d (ξ, μ_c, T) is the Fermi-Dirac distribution, ω is the radian frequency, e is the electron charge, k_B is the Boltzmann constant, T is temperature of Kelvin, $\hbar$ is the reduced Planck constant, $\Gamma=1/(2\tau)$ is the scattering rate, τ is the electron-phonon relaxation time, μ_c is the chemical potential, and ξ is the energy of electrons. At room temperature T=300 K, the intraband transition is dominant in the terahertz region compared with the interband transition. Therefore, the above Kubo equation can be simplified as a Drude-like form, which is

$$\sigma = \frac{je^2\mu_c}{\pi\hbar^2(\omega + j\tau^{-1})} \tag{5}$$

where the value of surface conductivity σ mainly depends on the three parameters, i.e., τ, μ_c and ω. According to the recently reported works from [35,36], τ and μ_c are set as 1 ps and 0.7 eV, respectively, in the simulation below.

3. Results and discussions

First, we study the absorption properties of the conventional periodic array using single square graphene ring deposited on the top layer under normal transverse electric (TE) and transverse magnetic (TM) polarized incidence as shown in the inset of Fig. 2(a). The single-resonant responses are generated with identical resonant frequency at 1.84 THz under both of TE and TM incidence, as demonstrated in Fig. 2(a). The single-resonant behavior can be explained by the Fabry–Pérot cavity theory, which has been qualitatively addressed in our previous works [21,37]. The polarization insensitivity is attributed to the symmetrical unit cell of the structure and the isotropic surface conductivity of graphene.

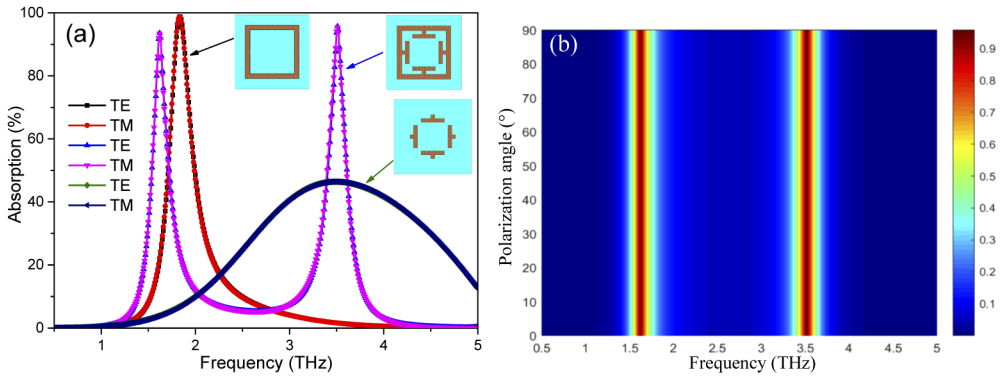

Fig. 2. (a) Absorption spectra of the traditional square graphene ring periodic array, only four T-shaped graphene strips periodic array, and proposed periodic array under normal TE and TM incident waves with the identical parameters (illustrated in Fig. 1). (b) Absorption spectra of the proposed periodic array for varied polarization angles.

Then, four T-shaped graphene strips are loaded to the square graphene ring without additionally increasing the size of MA device, which have two functions. The first one is to increase the effective length of the Fabry–Pérot resonator, resulting in a red shift of resonant frequency, as shown in Fig. 2(a). The second function is to generate a new resonance for achieving a dual-band MA. The absorption spectra of only four T-shaped graphene strips are illustrated in Fig. 2(a), where the absorption peak is located at 3.5 THz, although the absorption rate is low. When the four T-shaped graphene strips are connected with the square graphene ring, the absorption rate will be enhanced with the same operating frequency at 3.5 THz. Consequently, the proposed graphene based MA will create two nearly perfect absorption peaks at 1.62 and 3.5 THz with

Optics EXPRESS

corresponding absorptivity of over 94% for both TE and TM polarizations, as seen in Fig. 2(a). We further plot the absorption spectra with different polarization angles under normal incidence in Fig. 2(b), which demonstrates that the proposed dual-band MA has a polarization-insensitive property.

The dual resonant frequencies are mainly affected by the side length of the square graphene ring a and two distinct lengths of the T-shaped graphene strips l_1 and l_2. Figures 3(a)–3(c) depict the absorption spectra under different values of these three parameters. As a decreases from 2.9 μm to 2.3 μm, the resonant frequencies of the two absorption peaks are blue-shifted from 1.43 THz to 1.79 THz and from 3.33 THz to 3.69 THz, respectively, as shown in Fig. 3(a). The resonance frequencies and the side length a are almost in the inverse ratio [38]. For the lengths of the T-shaped graphene strips l_1 and l_2, when the values of them increase, the left absorption peak almost remains unchanged while the right one will be both red-shifted as demonstrated in Figs. 3(b) and 3(c), respectively. Therefore, the design procedure of the proposed dual-band MA is described as follows. First, tune the side length a to determine the left absorption band at the expected resonant frequency. Second, move the right absorption band to the desired resonant frequency by varying the parameters of the T-shaped graphene strips l_1 and l_2. Finally, slightly adjust the other parameters, i.e., w_1 and w_2, to optimize the peak absorption rates of the two bands. Furthermore, Fig. 3(d) shows that the peak absorption rates of the two bands will be tuned as the parameter τ changes, while the operating frequencies of the two bands remain unchanged. Accordingly, full width at half maximum (FWHM) can be adjusted by changing the electron-phonon relaxation time τ.

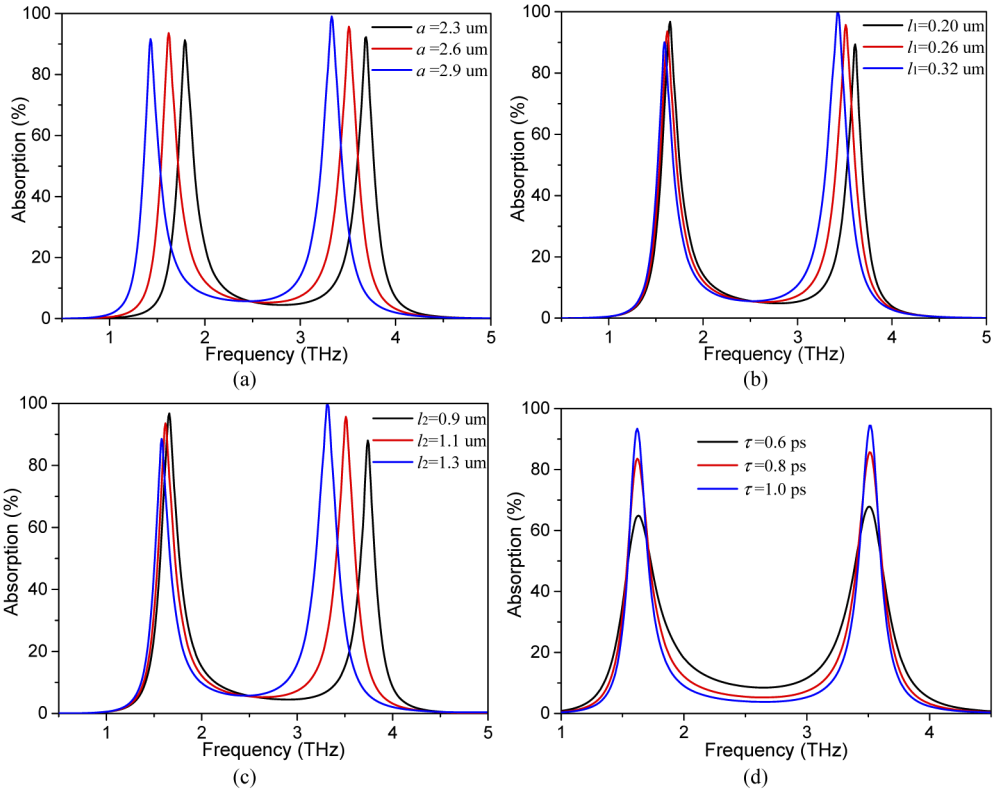

Fig. 3. Absorption spectra with different values of (a) parameter a, (b) parameter l_1 (c) parameter l_2 and (d) parameter τ under normal TE incident wave. The other default parameters are the same as illustrated in Fig. 1.

Optics EXPRESS

To better illustrate the physical mechanism of the proposed dual-band MA, the electric field intensity distributions are shown in Fig. 4. For the first absorption peak at 1.62 THz under TE polarization, the localized surface plasmon resonance is induced surrounding the perpendicular sides of square graphene ring and two perpendicular T-shaped graphene strips, as depicted in Fig. 4(a). This is because the high absorption rate at 1.62 THz is caused by the joint effect of square graphene ring and T-shaped graphene strips. In Fig. 4(b), the enhanced electric field is strongly concentrated along the two perpendicular T-shaped graphene strips. With the help of T-shaped graphene strips, the resonance occurs at 3.5 THz for the generation of the second absorption peak. The total absorption inside graphene can be calculated by the following equation [21],

$$A(\omega) = \omega\varepsilon'' \int_V |E|^2 dV \tag{6}$$

where V is the volume of graphene, $|E|$ is the electric field inside graphene, and ε'' is the imaginary part of graphene permittivity. The reflected energy from the gold mirror is suppressed by electromagnetic losses and the concentrated electric fields around graphene ring/strips dissipate in the lossy graphene, which contribute to the enhanced absorption inside graphene.

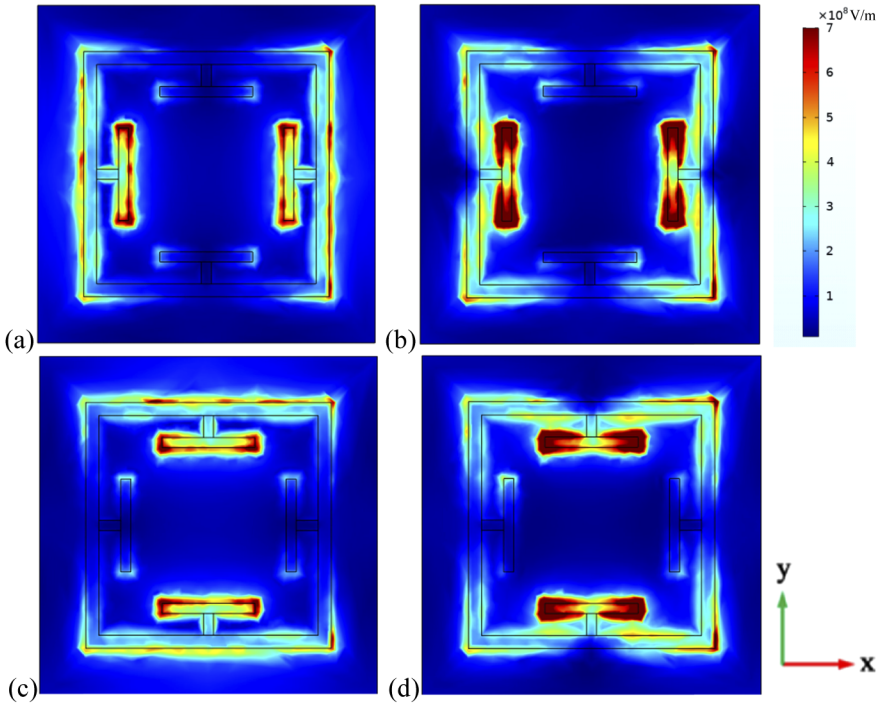

Fig. 4. Electric field intensity distributions of the MA unit cell in the top view at the frequencies of (a) 1.62 THz and (b) 3.5 THz under normal TE incidence. While (c) and (d) are those at 1.62 THz and 3.5 THz under normal TM incidence, respectively.

Figures 4(c) and 4(d) illustrate the electric field intensity distributions of the MA unit cell at 1.62 THz and 3.5 THz under normal TM polarized incidence, respectively, which are actually rotated 90° from those under TE polarization. Obviously, the proposed MA is of clear polarization independence, which validates the conclusion of polarization-insensitive property in Fig. 2.

The absorption spectra can be tuned by changing the geometric dimensions of the proposed graphene-based MA, which has been addressed before as shown in Fig. 3. However, the physical dimensions will be fixed once the absorber is finally fabricated and implemented, resulting in

Optics EXPRESS

hardly tuning its characteristics. Due to the active tunability of graphene according to Eq. (5), the performance of graphene-based MA can be manipulated to some extent by changing the chemical potential via chemical doping without changing the physical dimensions. The absorption tunability of the proposed graphene-based MA is illustrated in Fig. 5, where the parameter τ is still set as 1 ps.

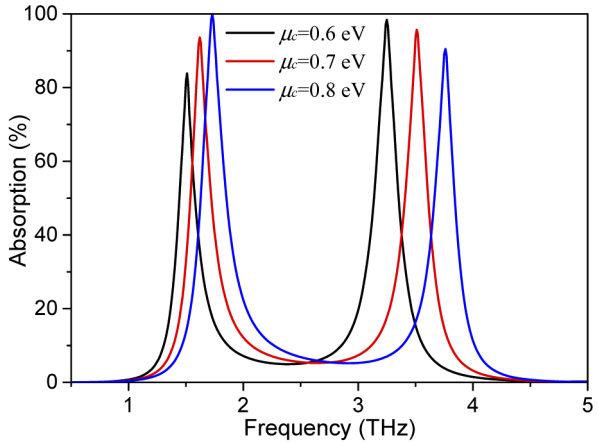

Fig. 5. Absorption spectra with different values of graphene chemical potential under normal TE incident wave.

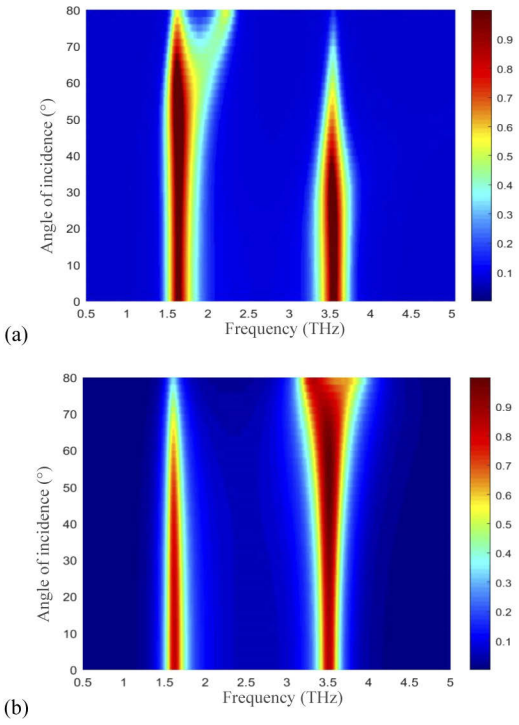

Fig. 6. Absorption of the proposed dual-band MA under different incident angles for (a) TE and (b) TM polarizations.

Optics EXPRESS

The above discussion is only based on normal incidence, but the robustness of optical response for non-normal incident angles is significant for terahertz absorbers, e.g., applications in sensing and detecting systems. Based on a series of simulations, the absorption stabilities of the proposed dual-band MA for both TM and TE polarizations are demonstrated in Fig. 6, as a function of frequency and angle of incidence. For TE polarization, the MA has two absorption peaks at 1.62 THz and 3.5 THz, respectively. The first one remains larger than 90% at 1.62 THz as the incident angle increases up to 80° as shown in Fig. 6(a). While the second absorption peak also remains the operating frequency unchanged at 3.5 THz when the incident angle is scanning from 0° to 80°, even though its magnitude has a dramatic drop under the incident angle of over 57°. For TM polarization, when the incident angle is smaller than 65°, the first absorption peak remains above 90% at 1.62 THz as shown in Fig. 6(b). On the other hand, the second absorption peak maintains over 95% at 3.5 THz when the incident angle is changed from 0° to 80°. As the angle of incidence increases to 50°, the bandwidth of the second absorption peak will be gradually broadened with the constant center frequency of 3.5 THz. Therefore, the absorption of the proposed MA can tolerate a wide incident angle for both TM and TE polarizations, which can be seen as a polarization-independent and angle-insensitive dual-band terahertz absorber.

4. Further extension to the tri-band absorber

In the discussions above, a novel structure using single layer graphene and only one patterned resonator in a periodic unit cell is proposed to design a tunable dual-band THz MAs. Based on this configuration, as shown in Fig. 7, four more T-shaped graphene strips are added to construct a new patterned graphene resonator for achieving triple resonant response in a certain spectral range, without additionally increasing the overall size of the periodic unit cell. The material properties of graphene, gold and Topas including the chemical potential as well as the periodicity of the MA p are the same as those in Fig. 1.

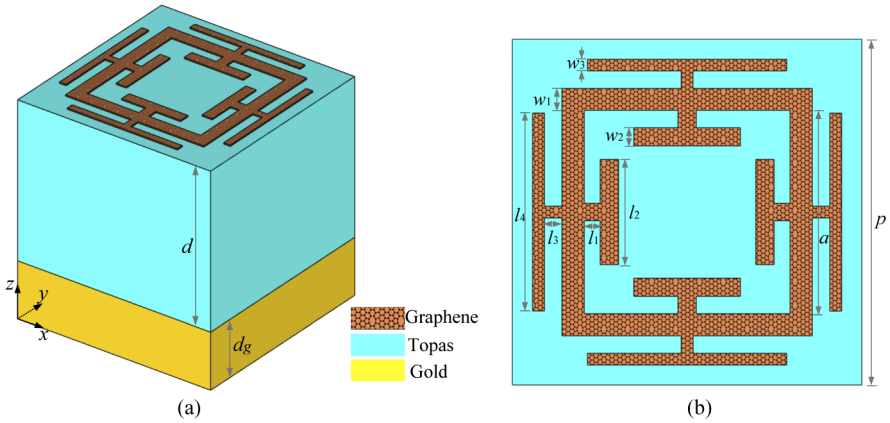

Fig. 7. (a) Perspective view and (b) top view of the graphene-based tri-band terahertz absorber, where w_1=0.21 μm, w_2=0.18 μm, w_3=0.12 μm, l_1 = 0.26 μm, l_2 = 1.1 μm, l_3 = 0.2 μm, l_4 = 2.5 μm, a=2.5 μm, p=4 μm, d=18 μm, and d_g=1 μm

Figure 8(a) illustrates the absorption spectra of the graphene-based tri-band terahertz absorber for TE and TM polarizations under normal incident wave. It has three absorption peaks at 1.21, 2.93, and 4 THz with corresponding absorptivity of over 85% for both TE and TM polarizations. Furthermore, the absorption spectra with different polarization angles under normal incidence are illustrated in Fig. 8(b). It demonstrates that the proposed tri-band MA is also of great polarization insensitivity. Figure 9 shows the absorption stabilities of the tri-band MA for both TM and TE

Optics EXPRESS

polarizations as the function of frequency and incident angle. For TE polarization, the MA has three absorption peaks at 1.21, 2.93 and 4 THz, respectively. The first one remains larger than 80% at 1.21 THz as the incident angle increases up to 70° as shown in Fig. 9(a). While the second

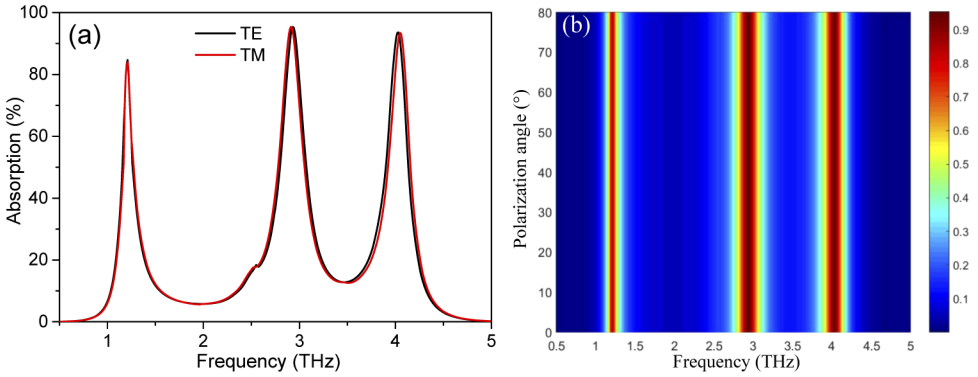

Fig. 8. Absorption spectra of the graphene-based tri-band terahertz absorber (a) for TE and TM polarizations, and (b) for varied polarization angles under normal incident wave, where $\tau = 1$ ps and $\mu_c = 0.7$ eV.

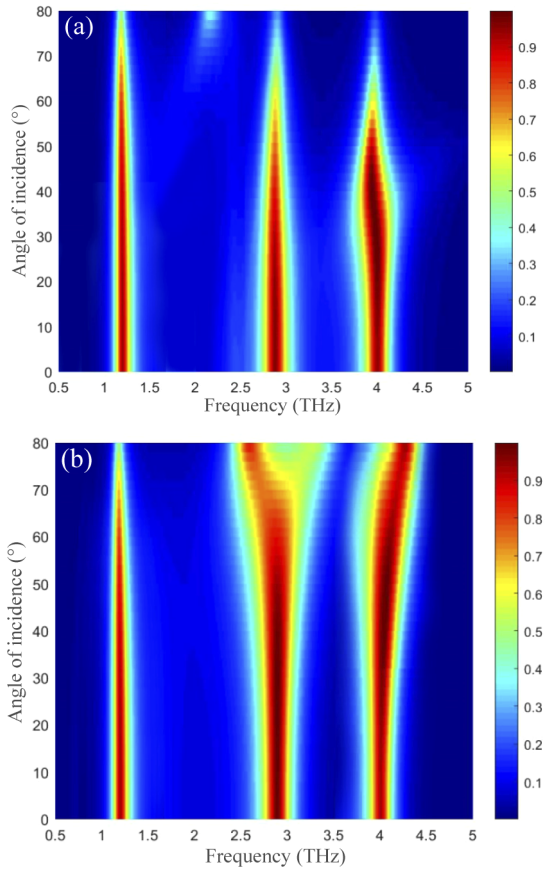

Fig. 9. Absorption of the proposed tri-band MA under different incident angles for (a) TE and (b) TM polarizations.

Optics EXPRESS

and third absorption peaks also remains the operating frequency and absorption rate unchanged when the incident angle is scanning from 0° to 55°. For TM polarization, the absorption rates are stable for the three bands even if the incident angle is scanned up to 75°, as shown in Fig. 9(b). The bandwidths of the second and third absorption peaks will be gradually broadened as the angle of incidence increases from 30° to 70°. Therefore, the absorption of this tri-band MA can also tolerate a wide incident angle for both TM and TE polarizations, which can be seen as a polarization-independent and angle-insensitive tri-band terahertz absorber. Moreover, the operating frequencies of these three absorption peaks can be also manipulated by adjusting the geometric dimensions and chemical potential of graphene.

5. Conclusions

In summary, a dual-band terahertz plasmonic absorber using monolayer square graphene ring with T-shaped graphene strips has been numerically demonstrated. The two absorption peaks can be tuned to the desired operating frequencies by varying the geometric dimensions of periodic array and chemical potential of graphene. Moreover, the proposed dual-band MA exhibits polarization independence and angular robustness for incident terahertz wave, which are of significant practicalities, such as the applications in sensing and detecting systems. Furthermore, the proposed structure can be extended to the design of tri-band absorber through adding four more T-shaped graphene strips on the previous patterned graphene resonator. This method does not increase an additional overall size of MA device but generates one more absorption peak. Therefore, our research work provides a new perspective for the design of various graphene-based tunable multi-band absorbers at terahertz, infrared or microwave frequencies.

Funding

Japan Society for the Promotion of Science (P19350).

Acknowledgments

The authors would like to thank Dr. Yijun Cai from Xiamen University of Technology, Xiamen, China, for technical advices and helpful discussion.

Disclosures

The authors declare that there are no conflicts of interest related to this article.

References

1. M. Tonouchi, "Cutting-edge terahertz technology," Nat. Photonics **1**(2), 97–105 (2007).
2. H. T. Chen, R. Kersting, and G. C. Cho, "Terahertz imaging with nanometer resolution," Appl. Phys. Lett. **83**(15), 3009–3011 (2003).
3. H.-J. Song and T. Nagatsuma, "Present and future of terahertz communications," IEEE Trans. Terahertz Sci. Technol. **1**(1), 256–263 (2011).
4. N. I. Landy, S. Sajuyigbe, J. J. Mock, D. R. Smith, and W. J. Padilla, "Perfect metamaterial absorber," Phys. Rev. Lett. **100**(20), 207402 (2008).
5. H. Tao, N. I. Landy, C. M. Bingham, X. Zhang, R. D. Averitt, and W. J. Padilla, "A metamaterial absorber for the terahertz regime: design, fabrication and characterization," Opt. Express **16**(10), 7181–7188 (2008).
6. K. Aydin, V. E. Ferry, R. M. Briggs, and H. A. Atwater, "broadband polarization-independent resonant light absorption using ultrathin plasmonic super absorbers," Nat. Commun. **2**(1), 517 (2011).
7. X. Shen, T. J. Cui, J. Zhao, H. F. Ma, W. X. Jiang, and H. Li, "Polarization-independent wide-angle triple-band metamaterial absorber," Opt. Express **19**(10), 9401–9407 (2011).
8. H. T. Chen, "Interference theory of metamaterial perfect absorbers," Opt. Express **20**(7), 7165–7172 (2012).
9. C. M. Watts, X. Liu, and W. J. Padilla, "Metamaterial electromagnetic wave absorbers," Adv. Opt. Mater. **24**(23), OP98–OP120 (2012).
10. X. Y. Liu, K. B. Fan, I. V. Shadrivov, and W. J. Padilla, "Experimental realization of a terahertz all-dielectric metasurface absorber," Opt. Express **25**(1), 191–201 (2017).

Optics EXPRESS

11. H. Chen, W. B. Lu, Z. G. Liu, J. Zhang, A. Q. Zhang, and B. Wu, "Experimental demonstration of microwave absorber using large-area multilayer graphene-based frequency selective surface," IEEE Trans. Microwave Theory Tech. **66**(8), 3807–3816 (2018).
12. L. Qi, C. Liu, and S. M. A. Shah, "A broad dual-band switchable graphene-based terahertz metamaterial absorber," Carbon **153**, 179–188 (2019).
13. J. Wang, Y. Jiang, and Z. Hu, "Dual-band and polarization-independent infrared absorber based on two-dimensional black phosphorus metamaterials," Opt. Express **25**(18), 22149–22157 (2017).
14. T. Guo and C. Argyropoulos, "Tunable and broadband coherent perfect absorption by ultrathin black phosphorus metasurfaces," J. Opt. Soc. Am. B **36**(11), 2962–2971 (2019).
15. Y. Jiang, W. Chen, and J. Wang, "Broadband MoS2-based absorber investigated by a generalized interference theory," Opt. Express **26**(19), 24403–24412 (2018).
16. J. Yan, Y. Zhang, P. Kim, and A. Pinczuk, "Electric field effect tuning of electron-phonon coupling in graphene," Phys. Rev. Lett. **98**(16), 166802 (2007).
17. L. Ye, Y. Chen, G. Cai, N. Liu, J. Zhu, Z. Song, and Q. H. Liu, "Broadband absorber with periodically sinusoidally-patterned graphene layer in terahertz range," Opt. Express **25**(10), 11223–11232 (2017).
18. Y. Zhao, B. Wu, B. Huang, and Q. Cheng, "Switchable broadband terahertz absorber/reflector enabled by hybrid graphene-gold metasurface," Opt. Express **25**(7), 7161–7169 (2017).
19. H. Xiong, Y. Wu, J. Dong, M. Tang, Y. Jiang, and X. Zeng, "Ultra-thin and broadband tunable metamaterial graphene absorber," Opt. Express **26**(2), 1681–1688 (2018).
20. L. Ye, X. Chen, J. Zhuo, F. Han, and Q. H. Liu, "Actively tunable broadband terahertz absorption using periodically square-patterned graphene," Appl. Phys. Express **11**(10), 102201 (2018).
21. Y. Cai and K. D. Xu, "Tunable broadband terahertz absorber based on multilayer graphene-sandwiched plasmonic structure," Opt. Express **26**(24), 31693–31705 (2018).
22. Y. Zhao, Q. Huang, H. Cai, X. Lin, H. He, T. Ma, and Y. Lu, "Dual band and tunable perfect absorber based on dual gratings-coupled graphene-dielectric multilayer structures," Opt. Express **27**(4), 5217–5229 (2019).
23. S.-X. Xia, X. Zhai, Y. Huang, J.-Q. Liu, L.-L. Wang, and S.-C. Wen, "Multi-band perfect plasmonic absorptions using rectangular graphene gratings," Opt. Lett. **42**(15), 3052–3055 (2017).
24. Z. Bao, J. Wang, Z.-D. Hu, A. Balmakou, S. Khakhomov, Y. Tang, and C. Zhang, "Coordinated multi-band angle insensitive selection absorber based on graphene metamaterials," Opt. Express **27**(22), 31435–31445 (2019).
25. Y. Liu, R. Zhong, J. Huang, Y. Lv, C. Han, and S. G. Liu, "Independently tunable multi-band and ultra-wide-band absorbers based on multilayer metal-graphene metamaterials," Opt. Express **27**(5), 7393–7404 (2019).
26. G. Deng, X. Song, S. A. Dereshgi, H. Xu, and K. Aydin, "Tunable multi-wavelength absorption in mid-IR region based on a hybrid patterned graphene-hBN structure," Opt. Express **27**(16), 23576–23584 (2019).
27. L. Ye, F. Zeng, Y. Zhang, and Q. H. Liu, "Composite graphene-metal microstructures for enhanced multiband absorption covering the entire terahertz range," Carbon **148**, 317–325 (2019).
28. F. Wang, S. Huang, L. Li, W. Chen, and Z. Xie, "Dual-band tunable perfect metamaterial absorber based on graphene," Appl. Opt. **57**(24), 6916–6922 (2018).
29. N. Hu, F. Wu, L.-A. Bian, H. Liu, and P. Liu, "Dual broadband absorber based on graphene metamaterial in the terahertz range," Opt. Mater. Express **8**(12), 3899–3909 (2018).
30. J.-S. Li, D.-X. Yan, and J.-Z. Sun, "Flexible dual-band all-graphene-dielectric terahertz absorber," Opt. Mater. Express **9**(5), 2067–2075 (2019).
31. https://topas.com/sites/default/files/files/topas_product-brochure_english.pdf
32. J. W. Suk, A. Kitt, C. W. Magnuson, Y. Hao, S. Ahmed, J. An, A. K. Swan, B. B. Goldberg, and R. S. Ruoff, "Transfer of CVD-grown monolayer graphene onto arbitrary substrates," ACS Nano **5**(9), 6916–6924 (2011).
33. M. Shirdel and M. A. Mansouri-Birjandi, "Broadband graphene modulator based on a plus-shaped plasmonic slot waveguide," Appl. Opt. **58**(30), 8174–8179 (2019).
34. G. W. Hanson, "Dyadic Green's functions and guided surface waves for a surface conductivity model of graphene," J. Appl. Phys. **103**(6), 064302 (2008).
35. J. Diaz, M. Morote, and J. Carrier, "Plane wave excitation detection of non-resonant plasmons along finite-width graphene strips," Opt. Express **21**(21), 24856–24872 (2013).
36. L. Ye, K. Sui, Y. Liu, M. Zhang, and Q. H. Liu, "Graphene based hybrid plasmonic waveguide for highly efficient broadband mid-infrared propagation and modulation," Opt. Express **26**(12), 15935–15947 (2018).
37. Y. Cai, K. D. Xu, N. Feng, R. Guo, H. Lin, and J. Zhu, "Anisotropic infrared plasmonic broadband absorber based on graphene-black phosphorus multilayers," Opt. Express **27**(3), 3101–3112 (2019).
38. W. J. Padilla, A. J. Taylor, C. Highstrete, M. Lee, and R. D. Averitt, "Dynamical electric and magnetic metamaterial response at terahertz frequencies," Phys. Rev. Lett. **96**(10), 107401 (2006).